Hindawi
Wireless Communications and Mobile Computing
Volume 2021, Article ID 4345622, 12 pages
https://doi.org/10.1155/2021/4345622

Research Article

Optimizing Energy Efficiency for Supporting Near-Cloud Access Region of UAV-Based NOMA Networks in IoT Systems

Huu Q. Tran,[1,2] **Ca V. Phan**,[1] **and Quoc-Tuan Vien**[3]

[1]*Ho Chi Minh City University of Technology and Education, Vietnam*
[2]*Industrial University of Ho Chi Minh City, Vietnam*
[3]*Middlesex University, UK*

Correspondence should be addressed to Huu Q. Tran; tranquyhuu@iuh.edu.vn

Received 13 May 2021; Accepted 15 September 2021; Published 6 October 2021

Academic Editor: L. J. García Villalba

Nonorthogonal multiple access (NOMA) and unmanned aerial vehicle (UAV) are two promising technologies for the wireless fifth generation (5G) networks and beyond. On the one hand, UAVs can be deployed as flying base stations to build line-of-sight (LoS) communication links to two ground users (GUs) and to improve the performance of conventional terrestrial cellular networks. On the other hand, NOMA enables the share of an orthogonal resource to multiple users simultaneously, thus improving the spectral efficiency and supporting massive connectivities. This paper presents two protocols, namely, cloud-based central station- (CCS-) based power-splitting protocol (PSR) and time-switching protocol (TSR), for simultaneous wireless information and power transmission (SWIPT) at UAV employed in power domain NOMA-based multitier heterogeneous cloud radio access network (H-CRAN) of Internet of Things (IoT) system. The system model with k types of UAVs and two users in which the CCS manages the entire H-CRAN and operates as a central unit in the cloud is proposed in our work. Closed-form expressions of throughput and energy efficiency (EE) for UAVs are derived. In particular, the EE is determined for the impacts of power allocation at CCS, various UAV types, and channel environment. The simulation results show that the performance for CCS-based PSR outperforms that for CCS-based TSR for the impacts of power allocation at the CCS. On the contrary, the TSR protocol has a higher EE than the PSR in the cases of the impact of various UAV types and channel environment. The analytic results match Monte Carlo simulations.

1. Introduction

Nonorthogonal multiple access (NOMA) has been recognized as one of the emerging technologies for the fifth generation (5G) network and beyond in the last decade [1–5]. Compared to conventional orthogonal multiple access (OMA), NOMA exhibits benefits such as low latency, high spectral efficiency (SE), high energy efficiency (EE), and fairness among users [6, 7]. Moreover, a huge number of devices are depicted that they will communicate with each other via wireless Internet connection in the future [8]. These provide a platform for the occurrence of the Internet of Things (IoT) concepts. The IoT concept has been defined by several study groups [9]. In IoT networks, the devices can be machines, sensors, smart phones, or any devices with wireless connection, thereby supporting massive object communication [10]. The key components which can realize the IoT concept in reality are sensor nodes [11, 12]. H-CRAN [13] is a new architecture which can enable users to utilize diverse services with low-cost operation, wide coverage, increased network architecture flexibility, and superior SE and EE by the employment of cloud computing and virtualization techniques [7, 14, 15]. H-CRAN is combined by a heterogeneous cellular network (HCN) [16] and a cloud radio access network (C-RAN) [17] and thus obtains the benefits of HCN and C-RAN. The baseband unit (BBU) pool is the main subsystem of H-CRAN architecture. Instead of utilizing the distributed processing at the base stations (BSs) like in the HCN, the BBU pool exploits a centralized signal processing mechanism to reduce the manufacturing and operating cost

[18, 19]. H-CRANs have drawn as a promising new technology and architecture in both industry and academia as well as platform of IoT. Therefore, H-CRAN has been considered the most important access method in the field of IoT [19]. In [20], a novel scheme for allocating the resource based on content sensing was proposed in 5G H-CRAN.

Normally, the nodes constrained by limited power want to prolong their lifetime need to harvest energy from other sources such as power grid, mechanical vibration, wind energy, solar energy, or radio frequency (RF) energy. The RF energy harvesting is one of the techniques which can be exploited in 5G networks [21]. These networks receive energy carried by RF signals and then convert to direct current (DC) energy for consuming and dedicating information transmission [22]. In RF EH relaying communication system, one of the relaying nodes is selected by the source to forward its information to the destination node. To perform this process, the relaying node harvests the energy from the RF-transmitted signal of the source to power up themselves [11]. By employing simultaneous wireless information and power transfer (SWIPT) mechanism, the relaying node not only harvests the energy but also receives the transmitted information from the RF signal of a source [21]. Thus, the SWIPT can be a potential technique to boost the EE and reliability in relay networks [23]. To harvest energy and process information at the relaying node, some protocols were proposed such as power-splitting-based relaying (PSR) and time-switching-based relaying (TSR) protocols along with decode-and-forward (DF) or amplify-and-forward (AF) mechanisms [3, 24]. In PSR, the EH and information processing (IP) are performed during the first phase while forwarding the information at the remaining time block. Otherwise, the TSR protocol divides the block time into three slots in which the EH occupies the first time block, the IP is in the second time slot, and then the information forwarding is in the last time slot of the block time. The combination of the power domain NOMA and SWIPT-based relaying communication was considered by many researchers [3, 25, 26]. Two critical techniques employed in NOMA include successive interference cancellation (SIC) and superposition coding [2]. The power allocation principle has more power for far user and less power for close user [3]. The relay node selection with the best conditions from the source helps obtain an optimized performance in the system [27–29]. In [30], a prioritization-based buffer-aided relay selection scheme which can seamlessly combine the NOMA and OMA transmission in the relay network was proposed. The proposed scheme considerably improved the data throughput at both low and high signal-to-noise ratio (SNR) regions. Thus, this scheme is attractive for cooperative NOMA in the IoT. In [31], two weighted-max-min and max-weighted-harmonic-mean optimal relay selection schemes were proposed for cooperative NOMA with fixed and adaptive power allocations at the relays. In [32], two relay selection algorithms with broadcasting, namely, buffer-aided (BA)-NOMA and BA-NOMA/OMA, were proposed for power-domain NOMA and hybrid NOMA/OMA. The simulation results demonstrated that the outage probability, average throughput, and average delay were improved.

1.1. Motivation and Contribution. In this paper, we propose a new system model along with two simultaneous EH and IP protocols based on PSR and TSR for relaying node in cooperative SWIPT NOMA-based H-CRAN of IoT network. We also propose an iterative algorithm to solve optimization issue for cloud-edge of downlink H-CRAN. Closed-form expressions of the performance metric in terms of throughput and EE are derived.

The main contributions of this paper are summarized as follows:

(i) A novel system model is proposed in this work which consists of one cloud-based central station (CCS) and k types of unmanned aerial vehicle (UAV) and operates based on cooperative non-orthogonal multiple access (C-NOMA) scheme

(ii) An employment of two SWIPT-based EH and IP protocols, namely, CCS-based PSR and CCS-based TSR, is exploited at the relaying node in this model

(iii) Closed-form expressions of throughput and EE are derived for the SWIPT NOMA system model

(iv) Impacts of power allocation, UAV types, and channel environment are investigated to realize the change of performance metric in the SWIPT NOMA H-CRAN

(v) The simulation results show that the EE of PSR is higher than that of TSR under different power allocation conditions at CCS. In contrast, the TSR protocol has a superior EE than PSR protocol under the impacts of UAV types and channel environment

1.2. Related Works. In [13], we proposed energy-efficient NOMA for wireless downlink in a multitier heterogeneous cellular network coordinated by a CCS, namely, H-CRAN. The proposed NOMA allocates different powers to different BS types depending on their relative distances to the CCS and the channel quality of the wireless links to enhance the spectrum efficiency and achievable throughput. Moreover, we investigated the employment of EH- and DF-based NOMA in a SWIPT system. Two PSR and TSR protocols are considered. In PSR and TSR protocols, the energy-constrained relay node uses apportion of the received power for EH, while the remaining energy is for IP [3–5]. In [33], a subchannel assignment and power allocation in multitier 5G H-CRANs were investigated to improve the system throughput. In [34], a power allocation was proposed for the wireless downlink in the H-CRAN. The EE of the practical NOMA-based H-CRAN was analyzed. This proposed scheme obtains a four times higher EE over the frequency division multiple access scheme. In [35], the EE and SE can be considerably enhanced by employing H-CRANs. In [36], a remote radio head selection algorithm along with a cross-layer EE-based resource allocation scheme was proposed to enhance the EE of the users in power domain NOMA H-CRAN to maximize the EE of the elastic users. In [37], the EE of an H-CRAN with several green remote radio heads powered by energy harvesting (EH) modules was studied. The maximum EE of the system was achieved by solving

Table 1: Symbol definition.

Symbol	Definition
$h_{k,i_k} \sim CN(0, \Omega_{k,ik})$	The complex flat coefficient in a wireless environment to the downlink channel between CCS and UAV_k
$n_{k,i_k} \sim CN(0,1)$	Additive white Gaussian noise (AWGN) at UAV_k with zero mean and variance of σ_k^2
$w_{Di} \sim CN(0,1)$	Additive white Gaussian noise (AWGN) at D_i with zero mean and variance of σ_i^2
$g_i \sim CN(0, \Omega_{Di})$	The channel coefficient of the UAV_{k,i_k} and D_i
P_{CCS}	Transmission power at the CCS
$\beta_{k,i_k}\left(0 < \beta_{k,i_k} < 1\right)$	The power-splitting ratio at the UAV_{k,i_k}
$E[.]$	Expectation operation
$E\left[\lvert h_{k,i_k}\rvert^2\right] = \frac{1}{d_{k,i_k}^{\nu_{k,i_k}}}$	Expectation operation of the flat channel coefficient of CCS $\longrightarrow$ UAV_k
$E\left[\lvert n_{k,i_k}\rvert^2\right] = \sigma_{k,i_k}^2$	Expectation operation of AWGN at UAV_k
ν_{k,i_k}	The path-loss of channel model
$x_i (i \in \{0,1\})$	The transmitted signal from the CCS to UAV_k
$E\left[\lvert x_i\rvert^2\right] = 1$	Expectation operation of x_i
$\alpha (0 < \alpha < 1)$	The time block fraction where UAV_{k,i_k} harvests the energy from the CCS
T	The total time block where the information is transmitted from the CCS to UAV_{k,i_k}
Θ_1	Power allocation coefficient for signal x_1
Θ_2	Power allocation coefficient for signal x_2
$\eta_{k,i_k}\left(0 < \eta_{k,i_k} \le 1\right)$	The energy conversion efficiency at the UAV_{k,i_k}
Macro	Macro UAVs
RRHs	Remote radio heads
Micro	Micro UAVs

the optimization problem, namely, the mixed integer nonlinear programming problem. The optimization problem was solved by the mesh adaptive direct search algorithm, and thus, the higher EE was obtained. The complexity and grid power consumption of the optimization problem is low.

In this paper, we combine our research works on H-CRAN, EH, IP, and DF-based using PSR and TSR protocols in a SWIPT C-NOMA system.

1.3. Organization. The rest of the paper is organized as follows. Section 2 presents the detail of the proposed system model and assumptions. Section 3 analyzes the performance parameters including throughput and energy efficiency of the system. Section 4 discusses the simulation results. Finally, Section 5 gives the main conclusions.

2. System Model

In the system model, to manage the whole H-CRAN, a CCS working as a central unit in the cloud is utilized. The distance between UAV_k and CCS is $d_k, k = 1, 2, 3, \cdots, K$. All UAV_k are assumed to connect to the CCS using wireless backhaul links with perfectly synchronous signals.

Table 1 lists the definition of the parameters used in the model and through the paper.

The CCS transmits the signal to users using multiple access points. Each UAV_{k,i_k} is equipped with a single antenna and operates in half duplex (HD) mode, where $i_k = 1, 2, \cdots, N_k$.

In our work, the best UAV selection case among UAVs is considered. Moreover, all UAVs are provided via wireless energy from the CCS instead of the conventional powers such as grid power and solar energy. The channels from the CCS to UAV_{k,i_k} and from UAV_{k,i_k} to two users D_1 and D_2 are flat Rayleigh block fading.

As shown in Figure 1, the shadowing impact and path loss of g_2 are less severe than g_1; the relation between Ω_{D1} and Ω_{D2} satisfies $\Omega_{D1} < \Omega_{D2}$.

2.1. Two EH Protocols at UAV_{k,i_k}. At the UAV_{k,i_k}, we consider two EH mechanisms including CCS-based PSR and CCS-based TSR protocols at the UAV_{k,i_k}.

2.1.1. The CCS-Based PSR Protocol for the Energy Harvesting at UAV_{k,i_k}ss. Figure 2 describes a diagram illustration of CCS-based PSR scheme for harvesting energy at UAV_{k,i_k} in the block time of T. The received signal power at UAV_{k,i_k} is indicated by P. It is assumed that the CCS sends the information to UAV_{k,i_k} in the half-block of T, while the information is transmitted from UAV_{k,i_k} to two users D_1 and D_2 in the remaining time of T.

The transmitted signal at the CCS is given by the following:

$$X_{\text{CCS}} = \left(\sqrt{\Theta_1 P_{\text{CCS}}} x_1 + \sqrt{\Theta_2 P_{\text{CCS}}} x_2\right). \quad (1)$$

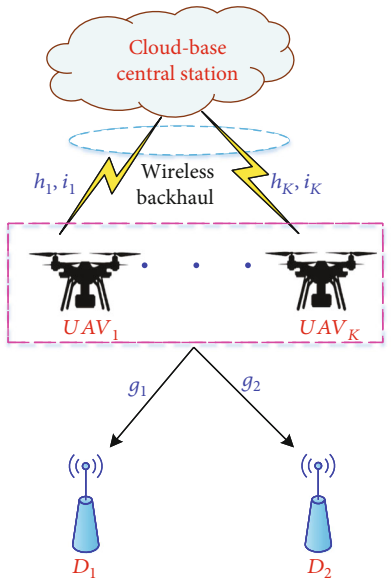

Figure 1: System model.

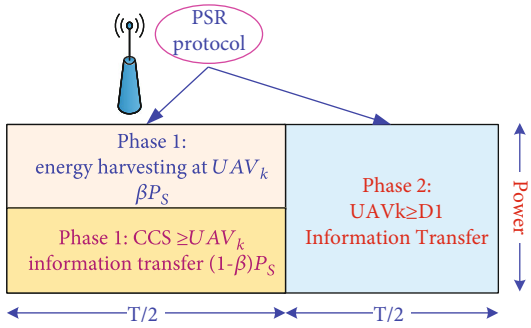

Figure 2: Diagram illustration of CCS-based PSR scheme.

We assume that UAV_{k,i_k} uses the harvested energy to forward the signal to D_1 and D_2. The power of transmitting-receiving circuit of UAV_{k,i_k} is negligible.

We can briefly describe the operation of the system as follows. Each communication block occupies two time slots. All blocks are normalized to unit. In the first slot time, the CCS transmits the superposed signal, i.e., $\sqrt{\Theta_1}x_1 + \sqrt{\Theta_2}x_2$. The expression of $(\Theta_1 + \Theta_2)$ satisfies to 1, and without loss of generality, it is assumed that $\Theta_1 \geq \Theta_2$. Applying superposition signal coding at the CCS as shown in the cooperative NOMA diagram [27], the observed signal at UAV_{k,i_k} is given by the following:

$$y_{k,i_k} = \sum_{k=1}^{K}\sum_{i_k=1}^{N_k} h_{k,i_k}\sqrt{P_{\text{CCS}}\Theta_i}x_i + w_{k,i_k}, \quad i \in \{0,1\}. \tag{2}$$

Based on the power-splitting architecture in [28] (Figure 3(b)), by employing the CCS-based PSR protocol, UAV_{k,i_k} divides the received energy into (i) harvested energy and (ii) energy for processing the information. The harvested energy at UAV_{k,i_k} can be computed by the following:

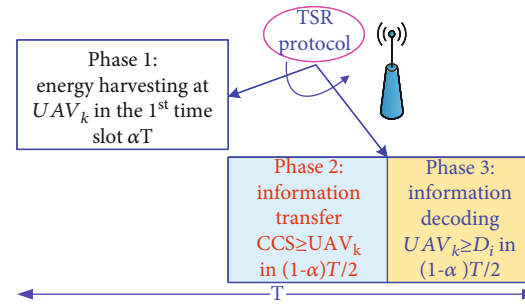

Figure 3: Diagram illustration of CCS-based TSR scheme.

$$E_{H,k,i_k}^{\text{PSR}} = \beta_{k,i_k}\eta_{k,i_k}P_{\text{CCS}}\left|h_{k,i_k}\right|^2\left(\frac{T}{2}\right). \tag{3}$$

The total harvested energy at UAV_{k,i_k} can be expressed by the following:

$$\begin{aligned} E_H^{\text{PSR}} &= \sum_{k=1}^{K}\sum_{i_k=1}^{N_k} E_{H,k,i_k}^{\text{PSR}} \\ &= \sum_{k=1}^{K}\sum_{i_k=1}^{N_k} \beta_{k,i_k}\eta_{k,i_k}P_{\text{CCS}}\left|h_{k,i_k}\right|^2\left(\frac{T}{2}\right). \end{aligned} \tag{4}$$

Assuming that the EH at each UAV_{k,i_k} is equal, the power of UAV_{k,i_k} for CCS-based PSR protocol can be determined from Equation (3) as follows:

$$\begin{aligned} P_{\text{UAV}}^{\text{PSR}} &= \frac{E_{H,k,i_k}}{(T/2)} \\ &= \frac{\beta_{k,i_k}\eta_{k,i_k}P_{\text{CCS}}\left|h_{k,i_k}\right|^2(T/2)}{(T/2)} \\ &= \beta_{k,i_k}\eta_{k,i_k}P_{\text{CCS}}\left|h_{k,i_k}\right|^2. \end{aligned} \tag{5}$$

It is assumed that β_{k,i_k} values at UAV_{k,i_k} as well as η_{k,i_k} at UAVs are equal. For simplicity, $0 < \eta \leq 1$ is named the EH efficiency. η depends on the energy conversion process from RF signal to DC in the receiver at UAV_{k,i_k}.

2.1.2. The CCS-Based TSR Protocol for the Energy Harvesting at UAV_{k,i_k}. Figure 3 illustrates the CCS-based TSR protocol of EH system. The block diagram for EH and information receiver in TSR protocol is based on [28] (Figure 2(b)). In the total time block T, αT is utilized for EH while $(1-\alpha)T$ is for forwarding the information. In the $(1-\alpha)T$, the first $(1-\alpha)T/2$ is dedicated for transmitting data from the CCS to UAV_{k,i_k} and the remaining $(1-\alpha)T/2$ is for forwarding data from UAV_{k,i_k} to user k. The harvested energy at UA V_{k,i_k} is given by the following:

$$E_{H,k,i_k}^{\mathrm{TSR}} = \alpha\eta_{k,i_k} P_{\mathrm{CCS}} \left|h_{k,i_k}\right|^2 T. \tag{6}$$

The total harvested energy at UAV_{k,i_k} can be expressed by the following:

$$\begin{aligned} E_H^{\mathrm{TSR}} &= \sum_{k=1}^{K} \sum_{i_k=1}^{N_k} E_{H,k,i_k}^{\mathrm{TSR}} \\ &= \sum_{k=1}^{K} \sum_{i_k=1}^{N_k} \alpha\eta_{k,i_k} P_{\mathrm{CCS}} \left|h_{k,i_k}\right|^2 T. \end{aligned} \tag{7}$$

Therefore, the power of UAV_{k,i_k} for CCS-based TSR protocol can be determined from Equation (6) as follows:

$$P_{\mathrm{UAV}}^{\mathrm{TSR}} = \frac{E_{H,k,i_k}^{\mathrm{TSR}}}{(1-\alpha)(T/2)} = \frac{2\alpha\eta_{k,i_k} P_{\mathrm{CCS}} \left|h_{k,i_k}\right|^2}{1-\alpha}. \tag{8}$$

In downlink power domain NOMA, SIC mechanism is exploited to decode the received signals at receivers, while superposition coding is applied to the code of the transmitted signals at transmitters. Thus, the SIC process is only considered at UAVs to achieve the best data forwarding as well as to allocate a higher power to D_1 and D_2 in our work. For instance, at UAV_{k,i_k}, the best UAV first decodes x_1 symbol by treating x_2 symbol as a noise and then performs SIC process to achieve x_2 signal. Therefore, the signal-to-interference-plus-noise ratio (SINR) for x_1 symbol and SNR for x_2 symbol are given by the following:

$$\gamma_{1,\mathrm{UAV}_k} = \frac{\Theta_1 \rho_{k,i_k} \left|h_{k,i_k}\right|^2}{\Theta_2 \rho_{k,i_k} \left|h_{k,i_k}\right|^2 + 1}, \tag{9}$$

$$\gamma_{2,\mathrm{UAV}_k} = \Theta_2 \rho_{k,i_k} \left|h_{k,i_k}\right|^2, \tag{10}$$

where $\rho_{k,i_k}\Delta = P_{\mathrm{CCS}}/w_{k,i_k}$ represents the transmit SNR. It is noted from Figure 1 that UAV_{k,i_k} processes signals x_1 and x_2 during the first time slot; then, the selected UAV sends the signal $\sqrt{P_{\mathrm{UAV}}}(\sqrt{\Theta_1}x_1 + \sqrt{\Theta_2}x_2)$ to two users D_1 and D_2 during the second time slot. Thus, the received signal at D_1 is combined by x_1, x_2 and noise and is given by the following:

$$y_{Di} = \sqrt{P_{\mathrm{UAV}}^X} g_i \left(\sqrt{\Theta_1}x_1 + \sqrt{\Theta_2}x_2\right) + w_{D_i}, \tag{11}$$

where $X \in \{\mathrm{PSR}, \mathrm{TSR}\}$ and g_i is the channel gain between the selected UAV and D_i.

From Equation (11), the SINR at D_1 is determined by applying SIC, i.e., D_1 decodes x_1 while treating x_2 as a noise, as follows:

$$\gamma_{1,D1} = \frac{\Theta_1 \rho_{\mathrm{UAV}}^X \left|g_1\right|^2}{\Theta_2 \rho_{\mathrm{UAV}}^X \left|g_1\right|^2 + 1}, \tag{12}$$

where $\rho_{\mathrm{UAV}}^X\Delta = P_{\mathrm{UAV}}^X/w_{D_i}$ denotes the transmitted SNR at D_i. Similarly, since both x_1 and x_2 are in D_2, it is necessary for SIC to decode its own symbol x_2. To perform SIC, D_2 decodes symbol x_1 by treating symbol x_2 as noise according to their priority power level and cancels x_2 using SIC to obtain symbol x_2. Therefore, the SINR for x_1 at D_2 is given by the following:

$$\gamma_{1,D2} = \frac{\Theta_1 \rho_{\mathrm{UAV}}^X \left|g_2\right|^2}{\Theta_2 \rho_{\mathrm{UAV}}^X \left|g_2\right|^2 + 1}. \tag{13}$$

The SNR for x_2 at D_2 decoded by its own D_2 is given by the following:

$$\gamma_{2,D2} = \Theta_2 \rho_{\mathrm{UAV}_{k,i_k}}^X \left|g_2\right|^2. \tag{14}$$

3. Performance Analysis

3.1. Throughput of the System. From Equation (2), for EH, the achievable throughput in bits/s at UAV_{k,i_k} can be given by the following:

$$R_{E_{k,i_k}} = W \log_2 \left(1 + \frac{\psi_E \rho_{\mathrm{UAV}}^X \left|h_{k,i_k}\right|^2}{\sum_{j=1}^{i_k-1} \psi_E \rho_{\mathrm{UAV},j}^X \left|h_{k,j}\right|^2 + \sigma_k^2}\right), \tag{15}$$

where ψ_E denotes the EH coefficient for CCS-based PSR and CCS-based TSR protocols and is expressed by the following:

$$\psi_E = \begin{cases} \beta\eta, \text{for CCS-based PSR,} \\ \dfrac{2\alpha\eta}{(1-\alpha)}, \text{for CCS-based TSR.} \end{cases} \tag{16}$$

The total throughput for EH in NOMA can be given by the following:

$$R_{E_{\mathrm{total}}} = \sum_{k=1}^{K} \sum_{i_k=1}^{N_k} W \log_2 \left(1 + \frac{\psi_E \rho_{\mathrm{UAV}}^X \left|h_{k,i_k}\right|^2}{\sum_{j=1}^{i_k-1} \psi_E \rho_{\mathrm{UAV},j}^X \left|h_{k,j}\right|^2 + \sigma_k^2}\right). \tag{17}$$

For IP, the achievable throughput in bits/s at UAV_{k,i_k} is expressed by the following:

$$R_{I_{i,i_k}} = W \log_2 \left(1 + \frac{\psi_I \rho_{\mathrm{UAV}}^X \left|h_{k,i_k}\right|^2}{\sum_{j=1}^{i_k-1} \psi_I \rho_{\mathrm{UAV},j}^X \left|h_{k,j}\right|^2 + \sigma_k^2}\right), \tag{18}$$

where W represents the channel bandwidth and ψ_I denotes the IP coefficient for CCS-based PSR and CCS-based TSR protocols and is given by the following

$$\psi_I = \begin{cases} \dfrac{(1-\beta)}{(2-\beta)}, \text{for CCS-based PSR,} \\ \dfrac{1}{2}, \text{for CCS-based TSR.} \end{cases} \tag{19}$$

The total throughput for IP in NOMA is given by the following:

$$R_{I_{\text{total}}} = \sum_{k=1}^{K} \sum_{i_k=1}^{N_k} W \log_2 \left(1 + \frac{\psi_I \rho_{\text{UAV}}^X \left| h_{k,i_k} \right|^2}{\sum_{j=1}^{i_k-1} \psi_I \rho_{\text{UAV},j}^X \left| h_{k,j} \right|^2 + \sigma_k^2} \right). \tag{20}$$

3.2. The Consumed Power Model. For the wireless downlink, the total consumed power includes UAVs, CCS, and backhaul powers.

3.2.1. The Consumed Power at a UAV. In a realistic cellular network, the consumed power of a UAV consists of the signal processing power at power amplifier (PA), transceivers, RF, and base band (BB) unit. Besides, the power attenuation caused by DC power, main source (MS), cooling, and the noneffectiveness of PA needs to be considered.

$P_k^{(\text{A})}$, $P_k^{(\text{RF})}$, and $P_k^{(\text{BB})}, k = 1, 2, \cdots, K$ represent the radiated output power at an antenna element, RF power, and BB power of a k-th type UAV, respectively. The consumed power of a k-th type UAV can be given by the following:

$$P_k^{(\text{C})} = N_k^{(\text{TRX})} \frac{\left(P_k^{(\text{A})} / \eta_k^{(\text{PA})} \left(1 - \alpha_k^{(\text{feed})} \right) \right) + P_k^{(\text{RF})} + P_k^{(\text{BB})}}{\left(1 - \alpha_k^{(\text{DC})} \right) \left(1 - \alpha_k^{(\text{MS})} \right) \left(1 - \alpha_k^{(\text{cool})} \right)}, \tag{21}$$

where $N_k^{(\text{TRX})}$ is the sequence number of transmitting/receiving, $\eta_k^{(\text{PA})}$ is the PA efficiency, $\alpha_k^{(\text{feed})}$ is the interforwarding loss, $\alpha_k^{(\text{DC})}$ is the loss of the DC-DC power, $\alpha_k^{(\text{MS})}$ is the loss of MS, and $\alpha_k^{(\text{cool})}$ is the cooling loss at the k-th type UAV.

3.2.2. The Backhauling Power. For downlink from the CCS to a UAV, the consumed power caused by wireless backhaul consists of the downlink interface power of wireless switching as well as general switching at the CCS. $P_k^{(\text{BH})}, k = \{1, 2, \cdots, K\}$ represents the backhauling power for downlink from the CCS to a k-th type UAV. Assuming that downlink interfaces and switching at UAV utilize the same type, $P_k^{(\text{BH})}$ is expressed by the following:

$$P_k^{(\text{BH})} = \frac{\omega_k P_{k,\max}^{(\text{SW})} + (1 - \omega_k) \left(A_{g_k}^{(\text{SW})} / A_{g_{k,\max}} \right) P_{k,\max}^{(\text{SW})}}{N_k^{(\text{INT})}} + P_k^{(\text{INT})}, \tag{22}$$

where $N_k^{(\text{INT})}$ is the number of interfaces for each switching, $P_{k,\max}^{(\text{SW})}$ is the maximum consumed power of the switching as all interfaces are in use, $P_k^{(\text{INT})}$ is the power for one interface in the general switching, $A_{g_k}^{(\text{SW})}$ is the flow-through switching node, and $A_{g_{k,\max}}$ is the maximization of the access flow of the switching at the k-th type UAV which can process. Here, ω_k is a critical component which effects on the consumed power for the general connection board of the switching.

In general, the total consumed power for H-CRAN downlink is given by the following:

$$P_{\text{tot}} = \sum_{k=1}^{K} \left[N_k \left(P_k^{(\text{C})} + P_k^{(\text{BH})} \right) + \sum_{i_k=1}^{N_k} P_{\text{UAV}}^X \right]. \tag{23}$$

3.2.3. Power Allocation for Wireless Downlink in H-CRAN. For simplicity, it is assumed that the power of interference at UAVs of a cell type is equal, i.e., $\sigma_{k,i_k}^2 = \sigma_{k,0}^2, \forall k = 1, 2, \cdots, K$, $i_k = 1, 2, \cdots, N_k$. We consider the power allocation for UAVs in the k-th cell type and represent the total transmitted power for UAVs in the k-th cell type and denote the total transmitted power at CCS for this k-th UAV type.

$$P_{k,\text{tot}} = \sum_{i_k=1}^{N_k} P_{\text{UAV}}^X. \tag{24}$$

Without loss of generality, it is assumed that $G_{k,1} > G_{k,2} > \cdots > G_{k,N_k}$, where G_{k,i_k} denotes the normalized channel gain of the link from CCS to UAV_k over the noise power. G_{k,i_k} can be expressed by the following:

$$G_{k,i_k} = \frac{E\left[\left| h_{k,i_k} \right|^2 \right]}{\sigma_{k,i_k}^2} = \frac{1}{d_{k,i_k}^{v_{k,i_k}} \sigma_{k,i_k}^2}. \tag{25}$$

The power allocated at UAVs in k-th type cells satifies $P_{k,1} < P_{k,2} < \cdots < P_{k,N_k}$. We denote $\lambda_{k,i_k}, i_k = 1, 2, \cdots, N_k - 1$, as a ratio of power allocation for $\text{UAV}_{k,i_{k+1}}$ and UAV_{k,i_k}. It means that

$$\lambda_{k,i_k} = \frac{P_{\text{UAV},i_k+1}^X}{P_{\text{UAV}}^X} = \frac{G_{k,i_k}}{G_{k,i_k+1}} = \frac{d_{k,i_k+1}^{v_{k,i_k+1}}}{d_{k,i_k}^{v_{k,i_k}}}. \tag{26}$$

According to recusive rule, Equation (25) is computed by the following:

$$\begin{aligned} P_{\text{UAV},i_k+1}^X &= \lambda_{k,i_k} P_{\text{UAV}}^X \\ &= \lambda_{k,i_k} \lambda_{k,i_k-1} P_{\text{UAV},i_k-1}^X \\ &= \prod_{j=1}^{i_k} \lambda_{k,i_k} P_{\text{UAV},1}^X. \end{aligned} \tag{27}$$

Similarly, the power allocation for UAV_k, N_k is computed by the following:

$$P_{k,N_k} = \prod_{j=1}^{N_{k-1}} \lambda_{k,j} P_{\text{UAV},1}^X. \tag{28}$$

At CCS, the total transmitted power for UAV in the k-th cell type can be obtained by the following:

$$P_{k,\text{tot}} = \sum_{i_k=1}^{N_k} \prod_{j=1}^{N_{k-1}} \lambda_{k,j} P_{\text{UAV},1}^{X}. \tag{29}$$

Therefore, the power for $\text{UAV}_{k,1}$ can be given by the following:

$$P_{k,1} = \frac{P_{k,\text{tot}}}{\sum_{i_k=1}^{N_k} \prod_{j=1}^{N_{k-1}} \lambda_{k,j}}. \tag{30}$$

Plugging Equation (29) into Equation (26), the power for each UAV, i.e., UAV_{k,i_k}, $i_k = (2, 3, \cdots, N_k)$, is computed by the following:

$$P_{\text{UAV}}^{X} = \frac{\prod_{j=1}^{i_{k-1}} \lambda_{k,j}}{\sum_{i_k=1}^{N_k} \prod_{j=1}^{i_{k-1}} \lambda_{k,j}} P_{k,\text{tot}}. \tag{31}$$

3.3. Efficiency Analysis and Optimization for Cloud-Edge in H-CRAN Downlink

3.3.1. Energy Efficiency of NOMA System. R and ξ denote the total throughput in bits/s and the EE in bits/J, respectively. The EE is defined as a ratio of the total throughput over the total consumed power in the entire network. It can be given by the following:

$$\xi \Delta = \frac{R}{P_{\text{tot}}}, \tag{32}$$

where P_{tot} is calculated by using Equation (23).

For NOMA H-CRAN downlink, the total EE is obtained by the following:

$$\xi = \frac{\sum_{k=1}^{K} \sum_{i_k=1}^{N_k} W \log_2 \left(1 + \left(\psi_I \rho_{\text{UAV}}^{X} \left|h_{k,i_k}\right|^2 / \sum_{j=1}^{i_k-1} \psi_I \rho_{\text{UAV},j}^{X} \left|h_{k,j}\right|^2 + \sigma_k^2\right) + \left(\psi_E \rho_{\text{UAV}}^{X} \left|h_{k,i_k}\right|^2 / \sum_{j=1}^{i_k-1} \psi_E \rho_{\text{UAV},j}^{X} \left|h_{k,j}\right|^2 + \sigma_k^2\right)\right)}{\sum_{k=1}^{K} \left[N_k \left(P_k^{(\text{C})} + P_k^{(\text{BH})}\right) + \sum_{i_k=1}^{N_k} \psi_E \rho_{\text{UAV}}^{X}\right]}. \tag{33}$$

Proof. See Appendix.□□ □

3.3.2. Optimization Problem for Supporting Near-Cloud Access Region Simultaneously for the Best UAV Selection and Transmitted EH to User. As presented in Equation (33), the efficiency of NOMA is affected by the quantity of cells of the different types. In reality, a huge number of cells causes low EE and significantly reduced throughput at cloud access region. For simplicity, it is assumed that the cell number, i.e., K, in H-CRAN is known and is constant. The aim of optimization issue is to find the maximum UAV of each cell type which this cell can be supported through constraints of the minimum throughput requirements at edge-cloud and the available limited power at the CCS. In the group of UAVs, it is only the best UAV which is selected to serve user D_i. This selection is based on the best channel selection from many downlink signal channels from UAVs. The optimization problem for UAVs of k-th cell type, $k = 1, 2, \cdots, K$, can be formulated by Equations (34) and (35)

$$\begin{aligned} &\max N_k \\ &\text{subject to} \sum_{i_k=1}^{N_k} P_{\text{UAV}}^{X} \le P_{k,\max}, \end{aligned} \tag{34}$$

$$W \log_2 \left(1 + \min \left(\frac{\psi_I \rho_{\text{UAV}}^{X} \left|h_{k,i_k}\right|^2}{\sum_{j=1}^{i_k-1} \psi_I \rho_{\text{UAV},j}^{X} \left|h_{k,j}\right|^2 + \sigma_k^2}, \frac{\psi_E \rho_{\text{UAV}}^{X} \left|h_{k,i_k}\right|^2}{\sum_{j=1}^{i_k-1} \psi_E \rho_{\text{UAV},j}^{X} \left|h_{k,j}\right|^2 + \sigma_k^2}\right)\right) \ge R_{k,\text{thre}}, \tag{35}$$

where $P_{k,\max}$ is the maximum power allocated for UAVs of the k-th cell type, $R_{k,\text{thre}}$ is the edge-cloud threshold throughput, and LHS of the constraint (Equation (35)) corresponding with the edge-cloud throughput, i.e., R_k, N_k, is given by Equation (18) with $i_k = N_k$. For simplicity, let $N_{k,\max}$ denote the maximum number of the k-th UAV type. To find $N_{k,\max}$, it can be performed by using the repeat algorithm as presented in a brief algorithm 1. The energy efficiency can be correspondingly determined by Equation (33) where $N_k = N_{k,\max}$.

4. Simulation Results

4.1. Simulation Parameters. The simulation parameters for evaluation scenarios of the SWIPT-based NOMA H-CRAN model are listed in Table 2.

4.2. The Performance for NOMA in Downlink H-CRAN

4.2.1. The Impacts of Power Allocation at CCS. First, we analyze the impacts of power allocation at the CCS on the performance of the proposed NOMA system in downlink H-CRAN. Figures 4–6 plot the EE of NOMA versus UAV number and different power levels at the CCS. Specifically, the power of 3 CCSs, i.e., $P\,(\text{CCS}) = 100\,;\,50\,;\,30$ kW, is simulated in urban cellular network model with $\nu = 2.4$. The distance from UAV to the CCS is within range of from 100 m to 8 km with a step of 200 m. Its corresponding channel gain is from 20 to 0 dB, while the attenuation factor is 0.5. Based on $R_{I_{\text{total}}}$, it is observed from Figure 4 that the

Table 2: Simulation parameters.

Parameters	Value
Number of cell types	3
Power consumption of macro-BS ($P_1^{(C)}$)	1350 W
Power consumption of RRH ($P_2^{(C)}$)	754.8 W
Power consumption of micro BS ($P_3^{(C)}$)	144.6 W
Power consumption of maximum switch	300 W
Power consumption of downlink interface	1 W
Interface number per switch	24
Maximum traffic of a switch	24 Gbps
Weighting factor	0.5
Transmission bandwidth	10 MHz
Energy harvesting efficiency (η)	0.8
Power splitting ratio (β)	0.7
Time block fraction (α)	0.7

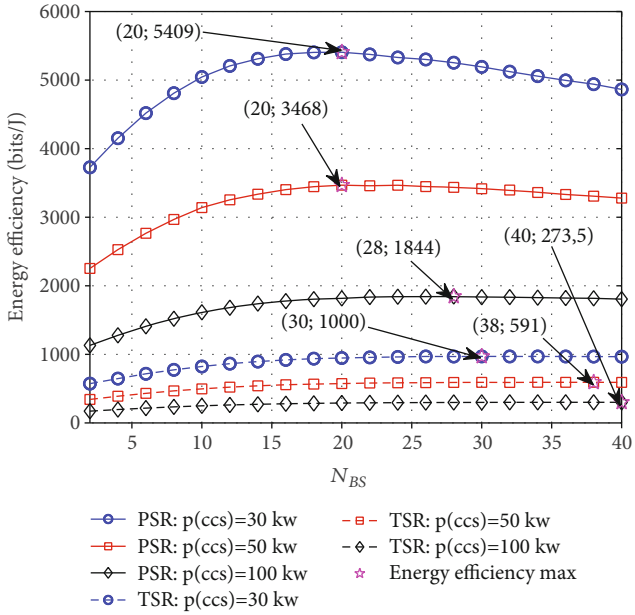

Figure 4: EE of the NOMA for IP ($R_{I_{\text{total}}}$) in CCS-based PSR and CCS-based TSR protocols versus UAV number with different power allocations.

EE for $P(\text{CCS}) = 30\,\text{kW}$ and $N_{\text{UAV}} = 18$, and CCS-based PSR protocol is the most superior at 5409 (bits/J), while this value for CCS-based TSR protocol is 979 (bits/J) at $N_{\text{UAV}} = 30$. Similarly, the EE for $P(\text{CCS}) = 50\,\text{kW}$ and $N_{\text{UAV}} = 22$, and CCS-based PSR protocol is the highest at 3468 (bits/J), while this value for CCS-based TSR is 591 (bits/J) at $N_{\text{UAV}} = 38$. In the case of $P(\text{CCS}) = 100\,\text{kW}$, the highest value of the EE for CCS-based PSR at $N_{\text{UAV}} = 28$ is 1844 (bits/J), while the highest value of the EE for CCS-based TSR at $N_{\text{UAV}} = 38$ is 309 (bits/J). This implies that the EE of CCS-based PSR is higher than that of CCS-based TSR. Similarly, based on $R_{E_{\text{total}}}$ and $(R_{I_{\text{total}}} + R_{E_{\text{total}}})$, Figures 5 and 6 show that the CCS-based PSR protocol achieves a higher EE than the CCS-based TSR.

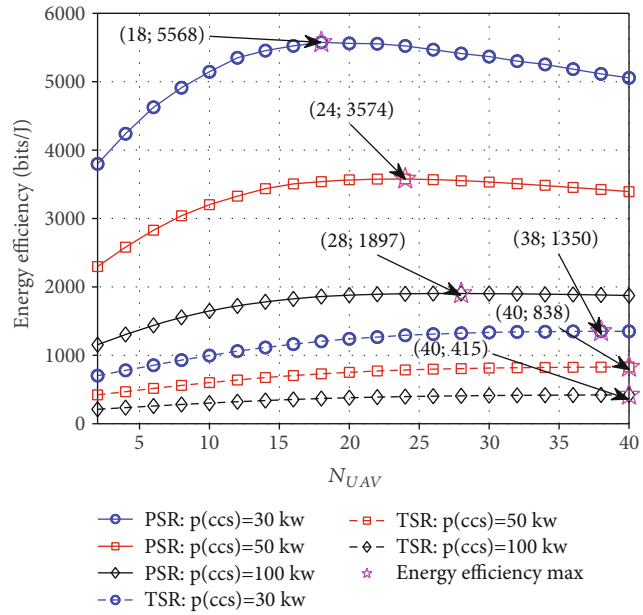

Figure 5: EE of the NOMA for EH ($R_{E_{\text{total}}}$) in CCS-based PSR and CCS-based TSR protocols versus UAV number with different power allocations.

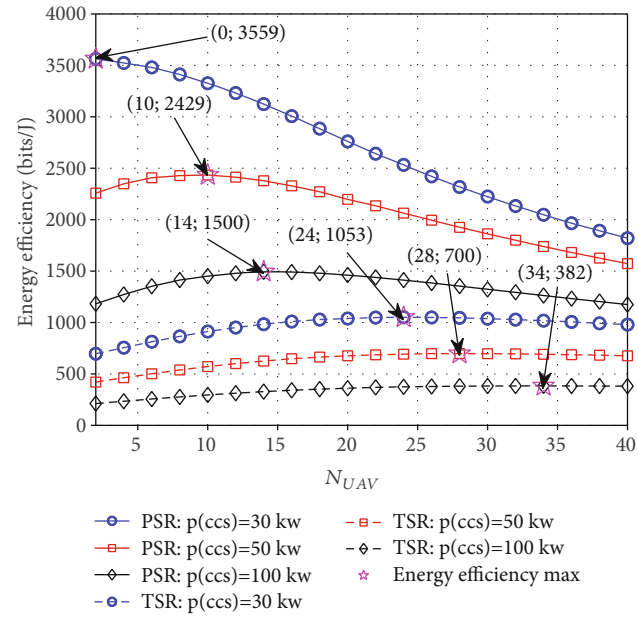

Figure 6: EE of the NOMA system ($R_{I_{\text{total}}} + R_{E_{\text{total}}}$) for CCS-based PSR and CCS-based TSR protocols versus UAV number with different power allocations.

4.2.2. The Impacts of UAV Types. Figures 7–9 describe the dependence of EE of NOMA in downlink H-CRAN on UAV types. Specifically, three types of UAVs such as macro-UAV, RRH, and micro-UAV are considered. The exploitation of mentioned UAVs shows the best EE performance. The exploitation of micro-UAV can achieve the highest EE performance for large networks, while this EE can be obtained for any UAV types for small networks. It is due to the fact that there is a difference in consuming

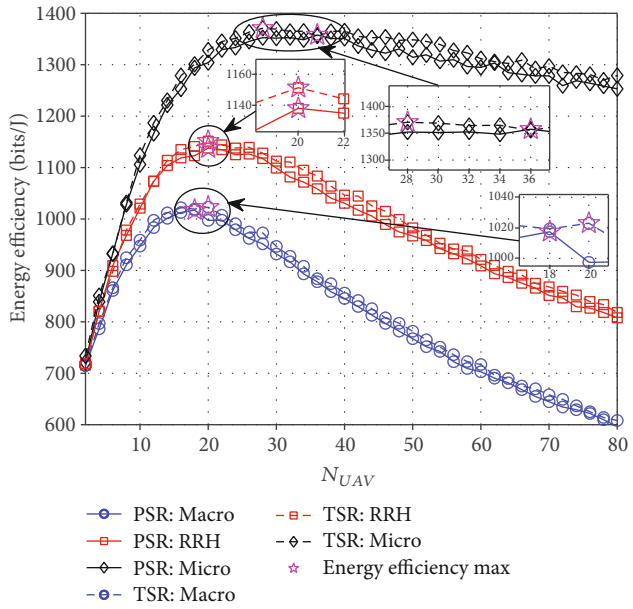

FIGURE 7: EE of the NOMA for IP ($R_{I_{\text{total}}}$) in CCS-based PSR and CCS-based TSR protocols versus UAV number with different UAV types.

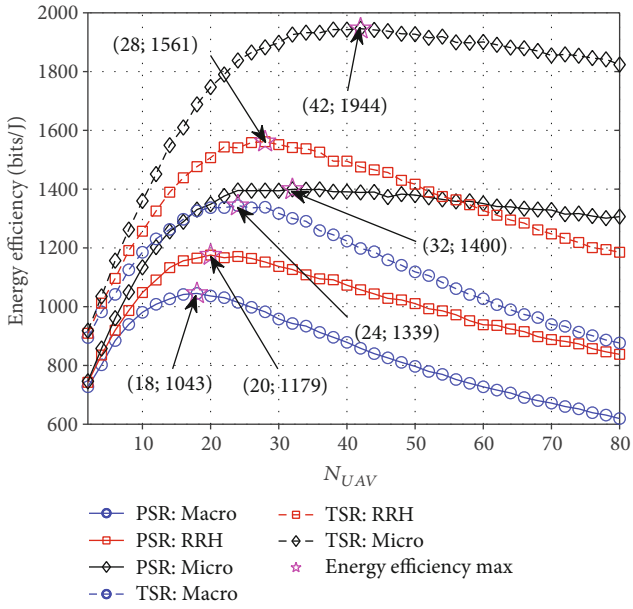

FIGURE 8: EE of the NOMA for EH ($R_{E_{\text{total}}}$) in CCS-based PSR and CCS-based TSR protocols versus UAV number with different UAV types.

power at the different types of UAVs. This agrees with the impacts of the types as well as the number of UAVs on the performance of H-CRAN. It is observed from Figure 7 that the highest EE value of CCS-based PSR for $R_{I_{\text{total}}}$-based micro-UAV is 1352 (bits/J) at $N_{\text{UAV}} = 32$, while this value for CCS-based TSR is 1373 (bits/J) at $N_{\text{UAV}} = 32$. In the case of RRH UAV, while the EE for CCS-based PSR achieves the highest value of 1133 (bits/J) at $N_{\text{UAV}} = 22$, that for CCS-based TSR obtains the highest value of 1152 (bits/J) at

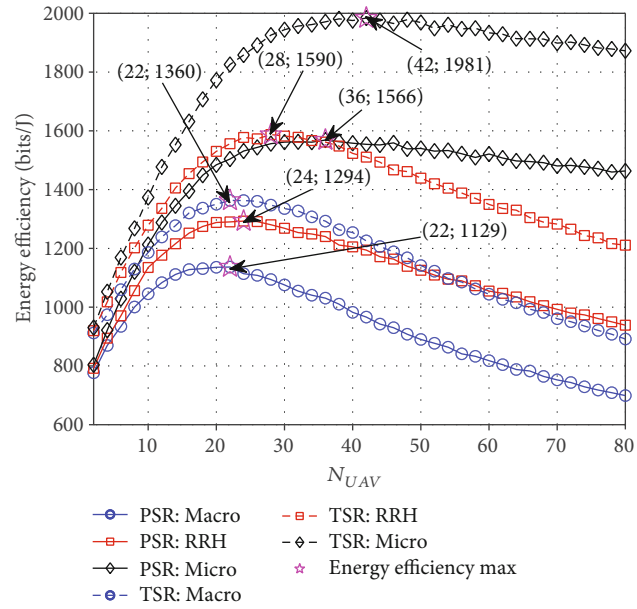

FIGURE 9: EE of the NOMA system ($R_{I_{\text{total}}} + R_{E_{\text{total}}}$) for CCS-based PSR and CCS-based TSR protocols versus UAV number with different UAV types.

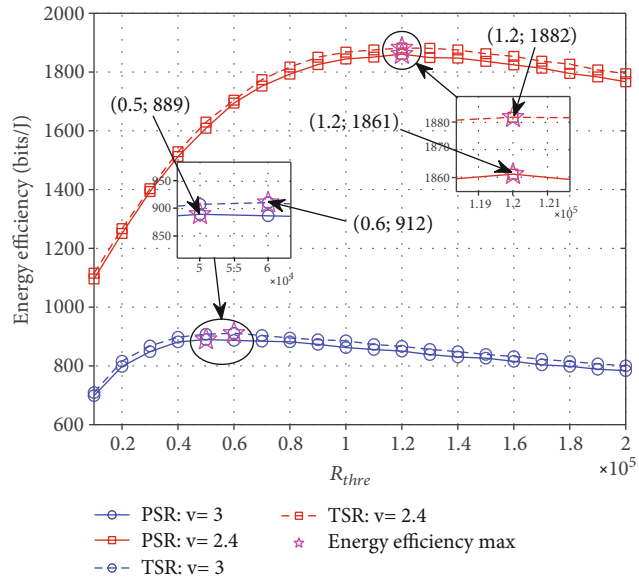

FIGURE 10: EE of the NOMA for EH versus cloud-edge throughput threshold with respect to various propagation path loss.

$N_{\text{UAV}} = 18$. Finally, in the case of macro-UAV, the highest EE for CCS-based PSR is 1025 (bits/J) at $N_{\text{UAV}} = 18$, and the highest EE for CCS-based TSR is 1152 (bits/J) at $N_{\text{UAV}} = 18$. This implies that the CCS-based TSR has a higher EE than CCS-based PSR. Similarly, based on $R_{E_{\text{total}}}$ and ($R_{I_{\text{total}}} + R_{E_{\text{total}}}$), Figures 5 and 7 show that the CCS-based TSR protocol achieves a higher EE than the CCS-based PSR.

4.2.3. The Impacts of Channel Environment. Figure 10 illustrates the EE with a maximum number of UAVs versus the threshold edge-cloud throughput in which urban and

shadowed urban environments are considered. From the figure, one can see that the maximum number of UAUs in both environments reduces as the edge-cloud throughput increases. Besides, Figure 10 also shows that the urban model can support two times UAVs, and its EE is higher than that for the shadowed urban model. Besides, in the case of $v = 3$, the highest EE for CCS-based PSR is 889 (bits/J) at $R_{\text{thre}} = 0.5 \times 10^5$ and the highest EE for CCS-based TSR is 912 (bits/J) at $R_{\text{thre}} = 0.6 \times 10^5$. In the case of $v = 2.4$, the CCS-based PSR achieves the best EE of 1861 (bits/J) at $R_{\text{thre}} = 1.2 \times 10^5$, while the CCS-based TSR achieves the best EE of 1882 (bits/J) at $R_{\text{thre}} = 1.2 \times 10^5$. In general, it can be concluded that the CCS-based TSR has a better EE than CCS-based PSR.

5. Conclusion

Two CCS-based PSR and CCS-based TSR protocols for EH and IP in cooperative SWIPT H-CRAN NOMA systems applied in IoT networks were presented in this paper. The closed-form expressions of throughput and the EE for UAVs were derived. The numerical simulation results show that the CCS-based PSR protocol achieved a higher EE as compared to CCS-based TSR protocol under the impacts of the power allocation at CCS. Specifically, the max EE of the NOMA system ($R_{I_{\text{total}}} + R_{E_{\text{total}}}$) for CCS-based PSR is higher than the CCS-based TSR protocol about 3.4 times, 3.5 times, and 3.9 times versus UAV number with $P_{\text{CCS}} = 30\,\text{kW}$, $P_{\text{CCS}} = 50\,\text{kW}$, and $P_{\text{CCS}} = 100\,\text{kW}$, respectively. Moreover, the CCS-based PSR protocol achieved a lower EE than the CCS-based TSR for the impact of UAV types and the impact of the channel environment. Specifically, the max EE of the NOMA system ($R_{I_{\text{total}}} + R_{E_{\text{total}}}$) for CCS-based PSR is lower than the CCS-based TSR protocol about 1.265 times, 1.229 times, and 1.205 times versus UAV number with micro-UAVs, RRHs, macro-UAVs, respectively. The analytic results matched the simulation results. For future work, we can develop the system using multiple antennas at two users D_1 and D_2 to enhance the performance of the system.

Appendix

The EE for EH is determined by substituting Equations (17) and (23) into Equation (32) and is obtained by the following:

$$\xi_E = \frac{\sum_{k=1}^{K}\sum_{i_k=1}^{N_k} W \log_2\left(1 + \left(\psi_E \rho_{\text{UAV}}^X \left|h_{k,i_k}\right|^2 / \sum_{j=1}^{i_k-1} \psi_E \rho_{\text{UAV},j}^X \left|h_{k,j}\right|^2 + \sigma_k^2\right)\right)}{\sum_{k=1}^{K}\left[N_k\left(P_k^{(\text{C})} + P_k^{(\text{BH})}\right) + \sum_{i_k=1}^{N_k} \psi_E \rho_{\text{UAV}}^X\right]}. \tag{36}$$

The EE for IP is determined by substituting Equations (20) and (23) into Equation (32) and is obtained by the following:

$$\xi_I = \frac{\sum_{k=1}^{K}\sum_{i_k=1}^{N_k} W \log_2\left(1 + \left(\psi_I \rho_{\text{UAV}}^X \left|h_{k,i_k}\right|^2 / \sum_{j=1}^{i_k-1} \psi_I \rho_{\text{UAV},j}^X \left|h_{k,j}\right|^2 + \sigma_k^2\right)\right)}{\sum_{k=1}^{K}\left[N_k\left(P_k^{(\text{C})} + P_k^{(\text{BH})}\right) + \sum_{i_k=1}^{N_k} \psi_E \rho_{\text{UAV}}^X\right]}. \tag{37}$$

Adding (36) and (37) and Equation (33) can be obtained. The proof is completed.

Data Availability

The data used to support the findings of this study are included in the paper.

Conflicts of Interest

The authors declare there is no conflict of interest in this manuscript.

Authors' Contributions

Huu Q. Tran is responsible for the conceptualization, methodology, software, formal analysis, and investigation. Huu Q. Tran is responsible for the data curation and writing the original draft preparation. Huu Q. Tran, Ca V. Phan, and Quoc-Tuan Vien are responsible for the validation and resources. Huu Q. Tran, Ca V. Phan, and Quoc-Tuan Vien are responsible for the writing, reviewing, and editing. Ca V. Phan and Quoc-Tuan Vien are responsible for the supervision.

Acknowledgments

This study was self-funded by the authors.

References

[1] S. T. Ooi, R. Ngah, and M. H. Azmi, "Full-duplex user-centric communication using non-orthogonal multiple access," *TELKOMNIKA Telecommunication Comput Electron and Control*, vol. 17, no. 5, pp. 2169–2178, 2019.

[2] S. R. Islam, N. Avazov, O. A. Dobre, and K. S. Kwak, "Power-domain non-orthogonal multiple access (NOMA) in 5G systems: potentials and challenges," *IEEE Communications Surveys Tutorials*, vol. 19, no. 2, pp. 721–742, 2017.

[3] H. Q. Tran, T. T. Nguyen, C. V. Phan, and Q. T. Vien, "Power-splitting relaying protocol for wireless energy harvesting and information processing in NOMA systems," *IET Communications*, vol. 13, no. 14, pp. 2132–2140, 2019.

[4] H. Q. Tran, C. V. Phan, and Q. T. Vien, "Power splitting versus time switching based cooperative relaying protocols for SWIPT in NOMA systems," *Physical Communication*, vol. 41, article 101098, 2020.

[5] H. Q. Tran, C. V. Phan, and Q. T. Vien, "Performance analysis of power-splitting relaying protocol in SWIPT based cooperative NOMA systems," *EURASIP Journal on Wireless Communications and Networking*, vol. 2021, no. 1, Article ID 1981, 2021.

[6] L. P. Liyn, H. Ghani, F. N. Roslim et al., "Ant-colony and nature-inspired heuristic models for NOMA systems: a review," *Telkomnika*, vol. 18, no. 4, pp. 1754–1761, 2020.

[7] M. Vaezi, Z. Ding, and H. V. Poor, *Multiple access techniques for 5G wireless networks and beyond*, Springer, Cham, 2019.

[8] L. Ericsson, *More Than 50 Billion Connected Devices*, vol. 14, White Paper, 2011.

[9] O. Elijah, T. A. Rahman, I. Orikumhi, C. Y. Leow, and M. H. D. N. Hindia, "An overview of Internet of Things," *Telkomnika*, vol. 18, no. 5, pp. 2320–2327, 2020.

[10] F. G. Abdulkadhim, Z. Yi, M. Khalid, and S. A. Waheeb, "A survey on the applications of IoT: an investigation into existing environments, present challenges and future opportunities," *Telkomnika*, vol. 18, no. 3, p. 1447, 2020.

[11] A. Rauniyar, P. Engelstad, and O. N. Østerb, "RF energy harvesting and information transmission based on power splitting and NOMA for IoT relay systems," in *2018 IEEE 17th International Symposium on Network Computing and Applications (NCA)*, pp. 1–8, Cambridge, MA, USA, 2018.

[12] J. M. Corchado, J. Bajo, D. I. Tapia, and A. Abraham, "Using heterogeneous wireless sensor networks in a telemonitoring system for healthcare," *IEEE Transactions on Information Technology in Biomedicine*, vol. 14, no. 2, pp. 234–240, 2010.

[13] H. Q. Tran, P. Q. Truong, C. V. Phan, and Q. Vien, "On the energy efficiency of NOMA for wireless backhaul in multi-tier heterogeneous CRAN," in *2017 International Conference on Recent Advances in Signal Processing, Telecommunications & Computing (SigTelCom)*, pp. 229–234, Da Nang, Vietnam, 2017.

[14] M. Peng, Y. Li, Z. Zhao, and C. Wang, "System architecture and key technologies for 5G heterogeneous cloud radio access networks," *Network*, vol. 29, no. 2, pp. 6–14, 2015.

[15] X. Wang, C. Cavdar, L. Wang et al., "Joint allocation of radio and optical resources in virtualized cloud RAN with CoMP," in *IEEE Global Communications Conference (GLOBECOM)*, pp. 1–6, Washington, DC, USA, 2016.

[16] S. Chinnadurai and D. Yoon, "Energy efficient MIMO-NOMA HCN with IoT for wireless communication systems," in *2018 International Conference on Information and Communication Technology Convergence (ICTC)*, pp. 856–859, Jeju, Korea (South), 2018.

[17] M. F. Hossain, A. U. Mahin, T. Debnath, F. B. Mosharrof, and K. Z. Islam, "Recent research in cloud radio access network (C-RAN) for 5G cellular systems - a survey," *Journal of Network and Computer Applications*, vol. 139, pp. 31–48, 2019.

[18] M. Peng, K. Zhang, J. Jiang, J. Wang, and W. Wang, "Energy-efficient resource assignment and power allocation in heterogeneous cloud radio access networks," *IEEE Transactions on Vehicular Technology*, vol. 64, no. 11, pp. 5275–5287, 2015.

[19] X. Zhang, M. Jia, X. Gu, and Q. Guo, "An energy efficient resource allocation scheme based on cloud-computing in H-CRAN," *IEEE Internet of Things Journal*, vol. 6, no. 3, pp. 4968–4976, 2019.

[20] J. Yang, J. Luo, F. Lin, and J. Wang, "Content-sensing based resource allocation for delay-sensitive VR video uploading in 5G H-CRAN," *Sensors*, vol. 19, no. 3, p. 697, 2019.

[21] T. N. Nguyen, M. Tran, P. Van-Duc, N. Hoang-Nam, and N. Thanh-Long, "Outage probability analysis of EH relay-assisted non-orthogonal multiple access (NOMA) systems over block rayleigh fading channel," *International Journal of Electrical and Computer Engineering*, vol. 9, no. 5, pp. 3607–3614, 2019.

[22] L. R. Varshney, "Transporting information and energy simultaneously," in *2008 IEEE International Symposium on Information Theory*, pp. 1612–1616, Toronto, ON, Canada, 2008.

[23] Z. Sun, L. Yang, J. Yuan, and D. W. K. Ng, "Physical-layer network coding based decoding scheme for random access," *IEEE Transactions on Vehicular Technology*, vol. 68, no. 4, pp. 3550–3564, 2019.

[24] A. A. Nasir, X. Zhou, S. Durrani, and R. A. Kennedy, "Relaying protocols for wireless energy harvesting and information processing," *IEEE Transactions on Wireless Communications*, vol. 12, no. 7, pp. 3622–3636, 2013.

[25] N. T. Do, D. B. da Costa, T. Q. Duong, and B. An, "A BNBF user selection scheme for NOMA-based cooperative relaying systems with SWIPT," *IEEE Communications Letters*, vol. 21, no. 3, pp. 664–667, 2017.

[26] Y. Yuan, Y. Xu, Z. Yang, P. Xu, and Z. Ding, "Energy efficiency optimization in full-duplex user-aided cooperative SWIPT NOMA systems," *IEEE Transactions on Communications*, vol. 67, no. 8, pp. 5753–5767, 2019.

[27] Z. Ding, H. Dai, and H. V. Poor, "Relay selection for cooperative NOMA," *IEEE Wireless Communications Letters*, vol. 5, no. 4, pp. 416–419, 2016.

[28] Z. Yang, Z. Ding, Y. Wu, and P. Fan, "Novel relay selection strategies for cooperative NOMA," *IEEE Transactions on Vehicular Technology*, vol. 66, no. 11, pp. 10114–10123, 2017.

[29] H. Lei, Z. Yang, K. H. Park et al., "Secrecy outage analysis for cooperative NOMA systems with relay selection schemes," *IEEE Transactions on Communications*, vol. 67, no. 9, pp. 6282–6298, 2019.

[30] M. Alkhawatrah, Y. Gong, G. Chen, S. Lambotharan, and J. A. Chambers, "Buffer-aided relay selection for cooperative NOMA in the Internet of Things," *IEEE Internet of Things Journal*, vol. 6, no. 3, pp. 5722–5731, 2019.

[31] P. Xu, Z. Yang, Z. Ding, and Z. Zhang, "Optimal relay selection schemes for cooperative NOMA," *IEEE Transactions on Vehicular Technology*, vol. 67, no. 8, pp. 7851–7855, 2018.

[32] N. Nomikos, T. Charalambous, D. Vouyioukas, G. K. Karagiannidis, and R. Wichman, "Hybrid NOMA/OMA with

buffer-aided relay selection in cooperative networks," *IEEE Journal of Selected Topics in Signal Processing*, vol. 13, no. 3, pp. 524–537, 2019.

[33] S. Ali, A. Ahmad, R. Iqbal, S. Saleem, and T. Umer, "Joint RRH-association, sub-channel assignment and power allocation in multi-tier 5G C-RANs," *IEEE Access*, vol. 6, pp. 34393–34402, 2018.

[34] Q. T. Vien, T. A. le, B. Barn, and C. V. Phan, "Optimising energy efficiency of non-orthogonal multiple access for wireless backhaul in heterogeneous cloud radio access network," *IET Communications*, vol. 10, no. 18, pp. 2516–2524, 2016.

[35] R. Q. Hu and Yi Qian, "An energy efficient and spectrum efficient wireless heterogeneous network framework for 5G systems," *IEEE Communications Magazine*, vol. 52, no. 5, pp. 94–101, 2014.

[36] A. Mokdad, P. Azmi, N. Mokari, M. Moltafet, and M. Ghaffari-Miab, "Cross-layer energy efficient resource allocation in PD-NOMA based H-CRANs: implementation via GPU," *IEEE Transactions on Mobile Computing*, vol. 18, no. 6, pp. 1246–1259, 2019.

[37] N. A. Chughtai, M. Ali, S. Qaisar, M. Imran, M. Naeem, and F. Qamar, "Energy efficient resource allocation for energy harvesting aided H-CRAN," *IEEE Access*, vol. 6, pp. 43990–44001, 2018.